


FULL PAPER

Open Access



Inflight calibration of the optical navigation camera for the extended mission phase of Hayabusa2

Manabu Yamada^{1*} , Toru Kouyama², Koki Yumoto³, Eri Tatsumi⁴, Naofumi Takaki³, Yasuhiro Yokota⁵, Tomokatsu Morota³, Naoya Sakatani⁵, Masahiko Hayakawa⁵, Moe Matsuoka⁶, Rie Honda⁷, Chikatoshi Honda⁸, Shingo Kameda⁹, Hidehiko Suzuki¹⁰, Yuichiro Cho³, Kazuo Yoshioka¹¹, Kazunori Ogawa¹², Kei Shirai¹³, Hirotaka Sawada⁶ and Seiji Sugita³

Abstract

After delivering its sample capsule to Earth, the Hayabusa2 spacecraft started its extended mission to perform a flyby of asteroid 2001 CC₂₁ in 2026 and rendezvous with asteroid 1998 KY₂₆ in 2031. During the extended mission, the optical navigation camera (ONC) of Hayabusa2 will play an important role in navigation and science observations, but it has suffered from optical deterioration after the spacecraft's surface contact with and sampling of asteroid Ryugu. Furthermore, the sensitivity of the telescopic camera (ONC-T) has continued to decrease for more than a year, posing a serious problem for the extended mission. These are problems that could potentially be encountered by other sample-return missions involving surface contact. In this study, we evaluated the long-term variation of ONC performance over the 6.5 years following the launch in 2014 to predict how it will perform during observations of the two target asteroids in its extended mission (6 and 11 years from the Earth return, respectively). Our results showed several important long-term trends in ONC performance, such as transmission, dark noise level, and hot pixels. During the long cruising period of the extended mission, we plan to observe both zodiacal light and exoplanet transits as additional science targets. The accuracy of these observations is sensitive to background noise level and stray-light contamination, so we conducted new test observations to search for the lowest stray light, which has been found to depend on spacecraft attitude. The results of these analyses and new test observations suggest that the Hayabusa2 ONC will be able to conduct cruising, flyby, and rendezvous observations of asteroids with sufficient accuracy.

Keywords Hayabusa2, Optical navigation camera, Extended mission, Calibration

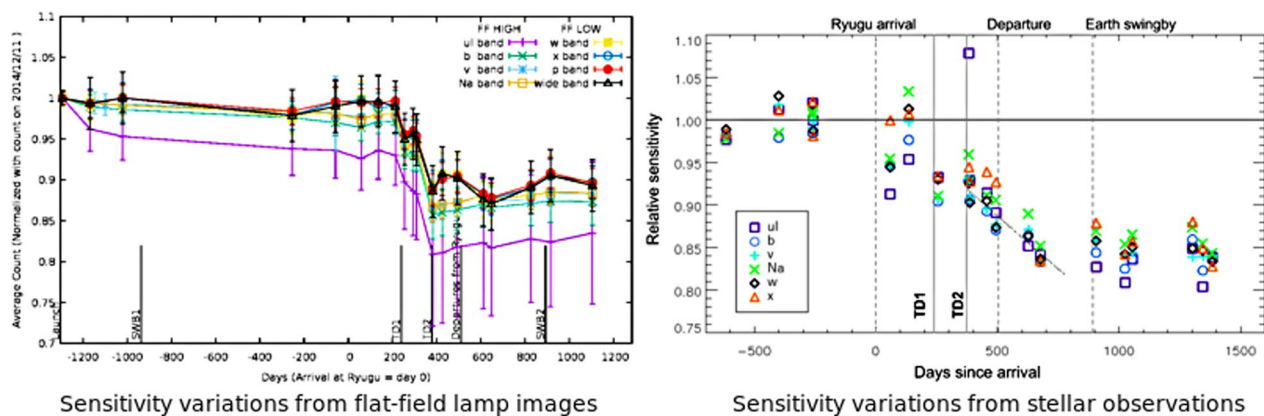
*Correspondence:

Manabu Yamada

manabu@perc.it-chiba.ac.jp

Full list of author information is available at the end of the article

Graphical Abstract



Introduction

After completing observations and sample collection of asteroid Ryugu from June 2018 to November 2019, Hayabusa2 successfully delivered Ryugu samples to Earth on December 6, 2020. Hayabusa2 then took off for another journey into deep space. JAXA is currently planning a flyby of the asteroid 2001 CC₂₁ in July 2026 and a rendezvous with asteroid 1998 KY₂₆ in July 2031 for the spacecraft's extended mission (Hirabayashi et al. 2021; Mimasu et al. 2022).

The optical navigation camera (ONC) onboard Hayabusa2 is a two-dimensional charge-coupled device (CCD) camera system consisting of three camera heads: a telescopic camera with seven color filters (ONC-T), and two monochrome wide-angle cameras (ONC-W1, W2) (Kameda et al. 2015, 2017; Suzuki et al. 2018; Tsumi et al. 2019). These cameras have so far observed spectroscopic and morphologic properties of asteroid Ryugu (e.g., Sugita et al. 2019; Watanabe et al. 2019; Tsumi et al. 2020; Yokota et al. 2021), dynamic processes during the touchdown (TD) sequences (Morota et al. 2020; Tachibana et al. 2022), and the artificially generated crater on Ryugu (e.g., Arakawa et al. 2020; Honda et al. 2021). The ONC will also be used to observe the shape, morphology, and spectra of the target asteroids during the extended mission. However, post-TD health-check observations have shown that the optical performance of the ONC has degraded, most likely because of the adhesion of surface materials kicked up during the two TDs on Ryugu's surface (Fig. 3.5c in Kouyama et al. 2021), leading to the concern that the optical performance may further degrade over the next 10 years.

Kouyama et al. (2021) obtained a degradation trend coefficient of $d_{TD2} = -0.000252 \text{ day}^{-1}$ from the

sensitivity time variation of ONC-T using observations of stars made during the second touchdown (TD2) between July 2019 and May 2020, assuming a linear degradation progression. However, if the sensitivity of ONC-T continues to degrade linearly with time, it will reach zero at around 4000 days (approx. 11 years) after TD2. Since this “zero-sensitivity” timing would be just before the arrival at asteroid 1998 KY₂₆ in 2031, the sensitivity degradation trend of ONC-T poses a serious problem. The main cause of sensitivity degradation is thought to be the adhesion of asteroid dust to the ONC-T optical system during TD. The mechanism behind the subsequent sensitivity reduction that has continuously occurred since then is not understood, so making a reliable prediction of sensitivity degradation has been difficult. Thus, empirical extrapolation based on actual sensitivity is the only way to make this prediction; we continued to monitor the degradation in ONC-T sensitivity after departing asteroid Ryugu.

To predict whether the sensitivity at the time of flyby and during arrival at the target asteroids will be high enough to conduct the observations necessary for achieving the mission goals of the extended mission, we estimate the sensitivity change using the calibration observation data taken with the flat-field (FF) lamps onboard ONC-T, and stellar observations accumulated from launch until May 2022, which is nearly 3 years after TD2. The extended period for the post-TD health check is much longer than a year, which our previous study (Kouyama et al. 2021) was based on, so we expected to be able to obtain a significantly more reliable prediction of the optical degradation trend now. If the predicted sensitivity at the time of flyby and arrival is high enough, then it will be needed for determining the optimal exposure time for observing the

new target asteroids. The objective is also to present updated information on sensitivity changes that will be necessary for future data archiving and reduction. Although detailed calibration of ONC-W1 and W2 has not been performed during cruising after the departure from Ryugu, we took a number of images using both W1 and W2 during the capsule delivery operation. The current status of ONC-W1 and W2 is inferred based on these images.

Sensitivity change of ONC-T

In the following section, we present a comparison among three independent results obtained from FF-lamp observations, stellar observations, and post-Earth swing-by lunar observations, as well as analyses of the sensitivity degradation of ONC and related phenomena. These three methods have their own pros and cons but are highly complementary to each other. Since the FF-lamp observation mode allows for a single light source to illuminate the entire field of view, it is easy to compare sensitivity over time. It is necessary, however, to take into account temperature changes and degradation of the lamp itself. In contrast, stellar observations are suitable for determining absolute sensitivity over time, but measurements can be made for an only limited number of pixels, and opportunities to observe the same star are limited. Lunar observations have an advantage over the other two observation methods, because the Lunar brightness is well-explored and the Moon can be used as a well-known light source. Thus, the Moon can provide both absolute and relative brightness over many more pixels in the CCD than stellar observations without affecting its temporal change. However, this calibration requires comparison with a lunar brightness model, which is much more complex than standard star data and has room for improvements. In addition, it has been known that the lunar calibration requires rather a strict geometrical condition, otherwise there could be large uncertainty (cf. Lach  rade et al. 2013).

Overall, the three calibration methods have different advantages and disadvantages. The results using the FF lamp were useful for examining the relative sensitivity of all pixels in the CCD. On the other hand, it is possible that the FF lamp was contaminated during the touch-down, and it may represent only a part of ONC-T optics due to its coverage (see Kouyama et al. 2021). Lunar calibration possibly provides a better result for measuring temporal variation in sensitivity. However, it requires a strict geometrical condition for accurate result, such as the same phase angle among observations, while it was not satisfied in ONC-T observations. In this study, it is

Table 1 Settings for performing health-check imaging with the FF lamp

Bands	Center wavelengths [nm]	Bandwidth [nm]	Exposure times for FF-lamp imaging [ms]	FF-lamp settings
ul	390.4	45	1049	High
b	479.7	25	524.8	High
v	549.0	28	131.2	High
Na	590.1	10	174.1	High
w	700.4	28	348.2	Low
x	858.9	42	65.6	Low
p	949.7	57	65.6	Low
Wide	775.0	850	5.44	Low

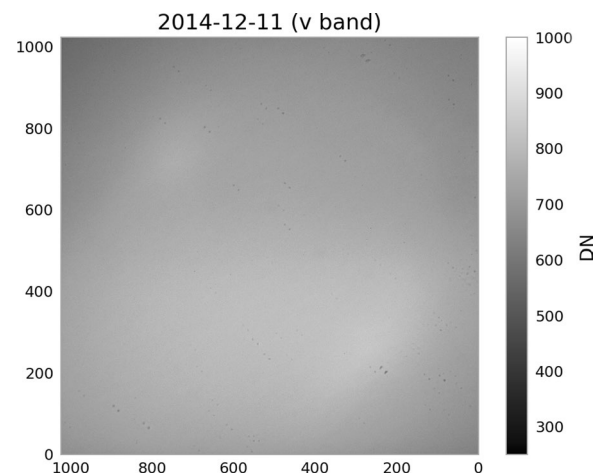


Fig. 1 FF-lamp image taken with the ONC-T v band in December 2014

better to trust the absolute value of the camera sensitivity estimated using the stars. Thus, we decided to use the stellar observations as nominal ones for the long term transmission monitoring.

Sensitivity variation of ONC-T observed with the FF lamp

The FF lamp is mounted in front of the optical system of the ONC-T and allows almost constant light to enter the photosensitive area of the CCD sensor, even in deep space. This health-check imaging with the FF lamp has been consistently performed with exactly the same sequence and exposure time as imaging during the ground test and cruising. Table 1 summarizes the exposure times and FF-lamp voltage settings for the health-check imaging for each band. By comparing the imaging data with this lamp turned on, we can estimate the sensitivity change of the entire CCD. Figure 1 shows the v-band FF-lamp image acquired in December 2014 immediately after launch. Since the two lamps are

installed diagonally, there are two areas that are brighter than the others in the field of view of ONC-T.

The FF-lamp voltage can be set to High or Low, which can be used for short wavelengths (ul (0.4 μm), b (0.48 μm), v (0.55 μm), and Na (0.59 μm) bands) and long wavelengths (w (0.70 μm), x (0.86 μm), p (0.95 μm), and wide bands), respectively. FF lamps at the High voltage setting are too bright for the w, x, and p bands, causing saturation, and those at the Low voltage setting are too dark for ul, b, v, and Na, leading to signal-to-noise ratios that are too low. As discussed by Kameda et al. (2017) and Tatsumi et al. (2019), the bias level, which is the offset of the signal of the ONC CCD, depends on the temperatures of the CCD, the electronic substrate of the camera head, and the ONC analog electric unit (ONC-AE). This temperature dependence of the bias level can be approximately compensated for by smear correction, which subtracts data taken at the minimum exposure time (0 s). The dark current noise caused by thermionic electrons, which depends highly on the CCD temperature, was reduced using images acquired at low CCD temperatures of below $-25\text{ }^{\circ}\text{C}$. Images with strong “radiator stray light”, whose intensities change greatly as a function of spacecraft attitude (Suzuki et al. 2018; Tatsumi et al. 2019), were not used for calibration analysis. At the Low voltage setting, FF-lamp brightness depends

linearly on the temperature of the ONC-AE, as reported by Kouyama et al. (2021). The ONC-AE temperature was not constant during the FF-lamp observations, because the ONC-AE was under a passive thermal control that depends on the temperature of the spacecraft. Thus, we linearly corrected the observed brightness to compensate for the effect of AE temperature deviation at $-6.8\text{ }^{\circ}\text{C}$, which was the ONC-AE temperature during the first FF-lamp observation conducted immediately after launch.

Figure 2 shows the change in the sensitivity of the ONC-T determined using FF-lamp images acquired from launch to July 2021. The value on the vertical axis is the average of the count values in all pixels of the CCD divided by the value immediately after launch. FF-lamp images taken around a year after launch indicate that the ul band signal experienced a large (approx. 5%) drop. Subsequently, there was less than a 2% change at most in all bands until arrival at Ryugu in June 2018. There was a 4–5% drop after the first touchdown (TD1) in February 2019, and a 6–7% drop after TD2 in July 2019. These post-TD decreases appear to be greater for shorter wavelength bands. After departure from Ryugu in November 2019, there was no significant decrease, and there may even be a small increase.

Health-check observations using FF lamps after TD operations also showed that ONC-T had some change

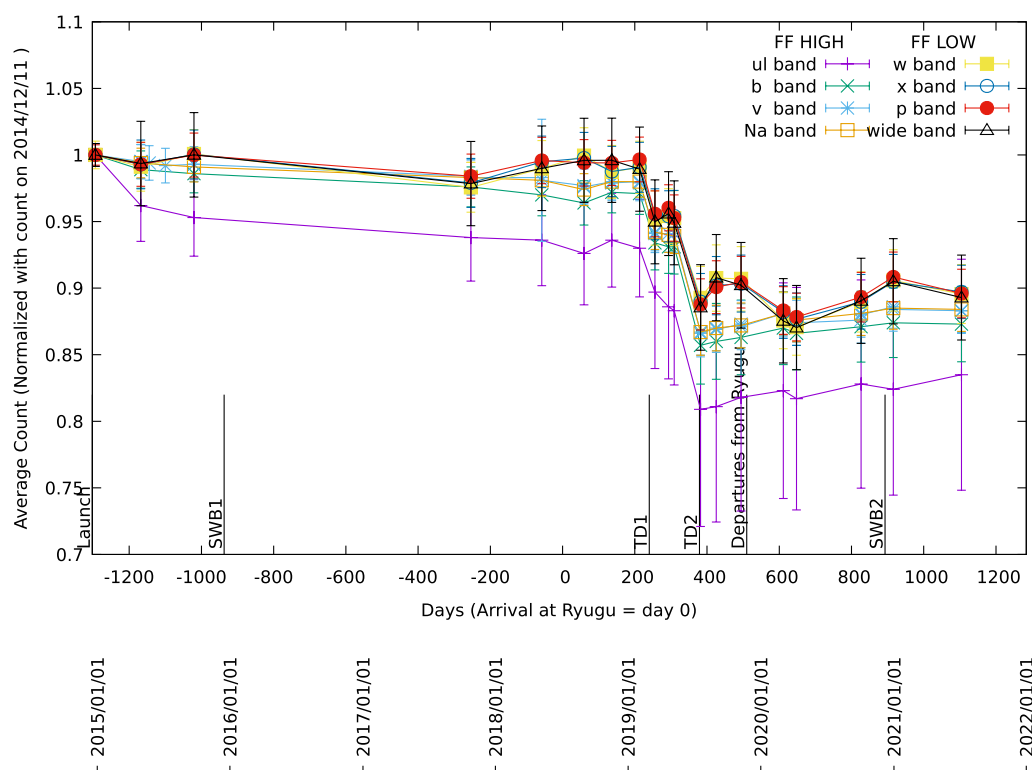


Fig. 2 History of ONC-T sensitivity changes from launch to July 2021

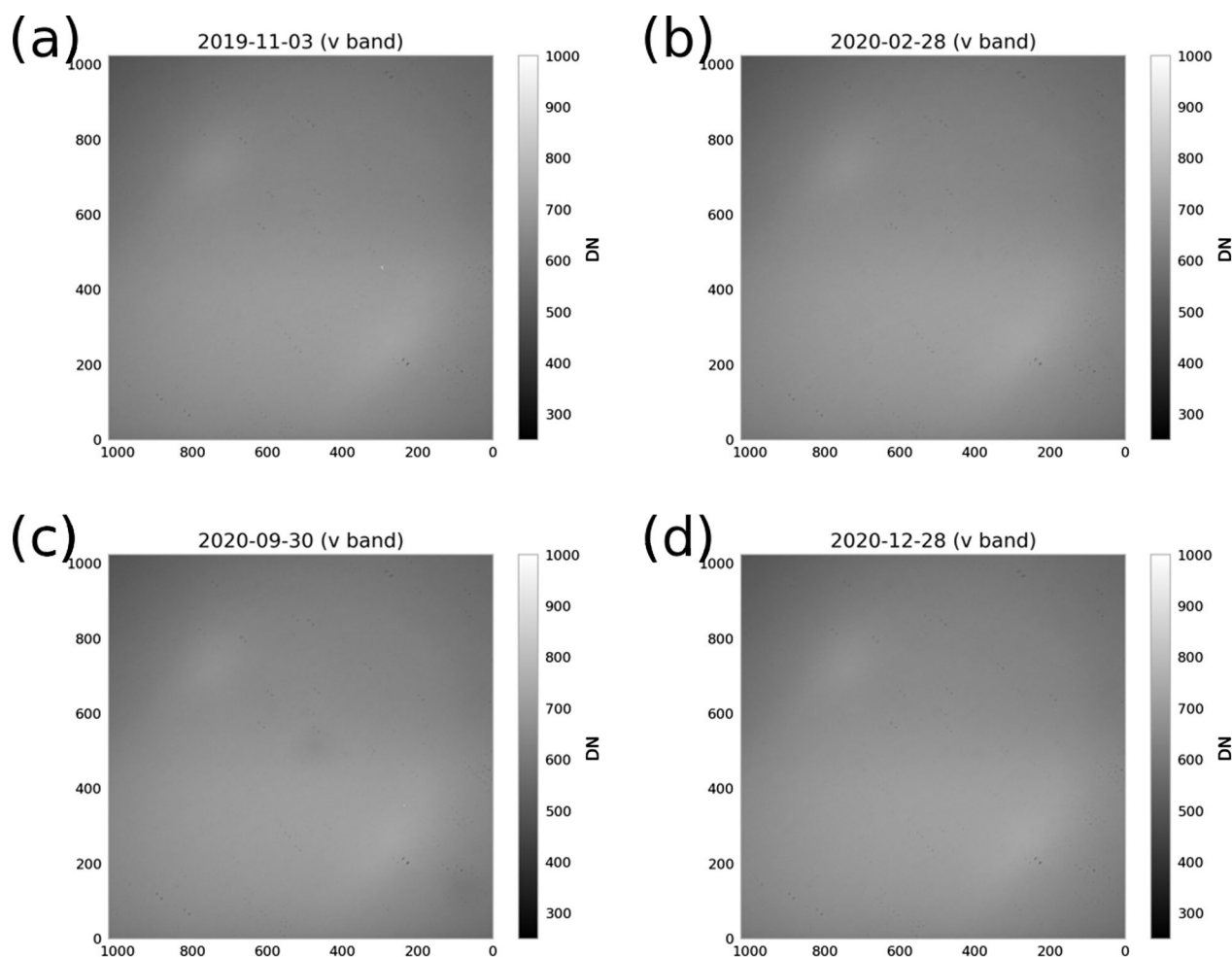


Fig. 3 ONC-T v-band FF-lamp images acquired from just before departure from Ryugu (November 3, 2019) to after capsule re-entry (December 28, 2020). Dark areas only appeared on September 30, 2020 near the center and lower right of the image

in lens contamination that we had not seen before. Figure 3a shows an image of the FF lamp acquired prior to the departure from Ryugu in November 2019. This image is not significantly different from the one taken immediately after launch (Fig. 1). The next FF-lamp image acquired in February 2020 (Fig. 3b) did not have any differences either. In the image taken in September 2020 (Fig. 3c), however, dark areas appeared near the center and lower right of the field of view. Subsequently in December 2020, these dark areas were no longer visible in the FF-lamp image after the return to Earth (Fig. 3d). Figure 4 emphasizes these dark areas by taking the ratio of the September 2020 FF-lamp image to that taken in November 2019. This black area was about 5% lower than normal. Since these dark areas appeared in all bands of the image and the silhouettes of the spots were blurred, which indicate that these causal particles are emplaced not directly on the ONC-T sensor. It is suspected that something was deposited either on the optics other

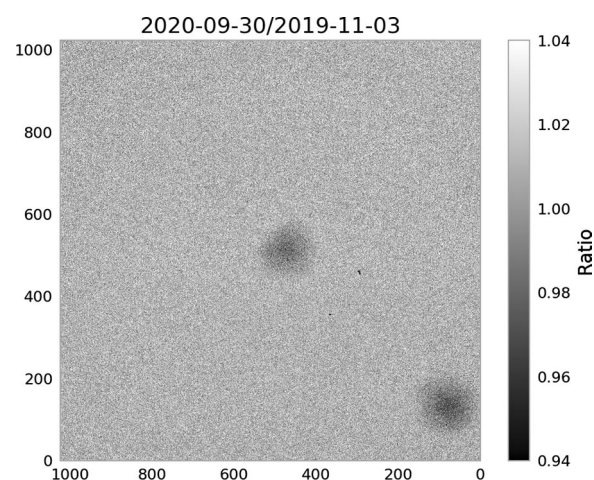


Fig. 4 Dark areas are emphasized by taking the ratio of the FF-lamp image taken on September 30, 2020, in which the dark areas appeared, and the FF-lamp image taken on November 3, 2019, which was acquired just before departure from Ryugu

than the filter. This was the first time that such a change occurred in the FF-lamp image since the launch of Hayabusa2 in 2014.

It has been highly uncertain what mechanism led to this phenomenon, but the following three scenarios could be possible. First, we think it is possible that a particle, which was small but large enough for generating a dark spot in ONC-T image frame, came from inside the baffle. This would be the same reason for the long-term degradation trend seen after the second touchdown; this might be due to motion of powder-like fine dust particles, that stuck inside the baffle at the touchdown events.

Dusts from Hayabusa2 body might also be a candidate for the dark spot. Because it requires a really special dust trajectory that passed through a small aperture of the ONC-T baffle, its possibility should be small. However, we cannot discard this possibility, since many trajectories of particles likely from Hayabusa2 body have been observed in ONC-T images.

Another possibility is condensation and evaporation of volatile material as an important candidate for the dark spot at the coldest point of the ONC-T optics. During the cursing phase, we have conducted several observations at different spacecraft attitudes, which would change temperature distribution on Hayabusa2, including the ONC-T system. In particular, the long baffle might be the most affected component. Such temperature variation might have led to evaporation of volatile from dusts

inside the baffle and/or around ONC-T optics, and then condensation on the ONC-T front lends.

Figures 5 and 6 show the temperature histories of the CCD sensor and the ONC-T optics before and after these dark areas appeared. The CCD sensor is cooled by a radiator that keeps its temperature low (-20°C or lower) except in special cases. There is no significant difference in the CCD temperature before and after the dark areas appeared. On the other hand, the optical system of the ONC-T fluctuates between low temperatures (approx. -20°C), which might lead to volatile condensation, during the storage mode and high temperatures (approx. $+20^{\circ}\text{C}$), which might lead to evaporation, during the imaging mode. The temperature of the optical system was kept at -20°C for around 5 months until just before imaging in September 2020, when the dark areas were observed. It was then kept at higher temperatures (approx. $+20^{\circ}\text{C}$) until the next FF-lamp imaging 3 months later.

Although the optics had been kept at low temperatures for more than 5 months during the period between launch and asteroid departure, these dark areas never appeared. The fact that they appeared when the optical system was kept at low temperatures for a long period of time after departing Ryugu suggests that outgas released from asteroid-derived materials adhered to the ONC-T and its surroundings during TD. No such spots appeared in the FF-lamp images taken

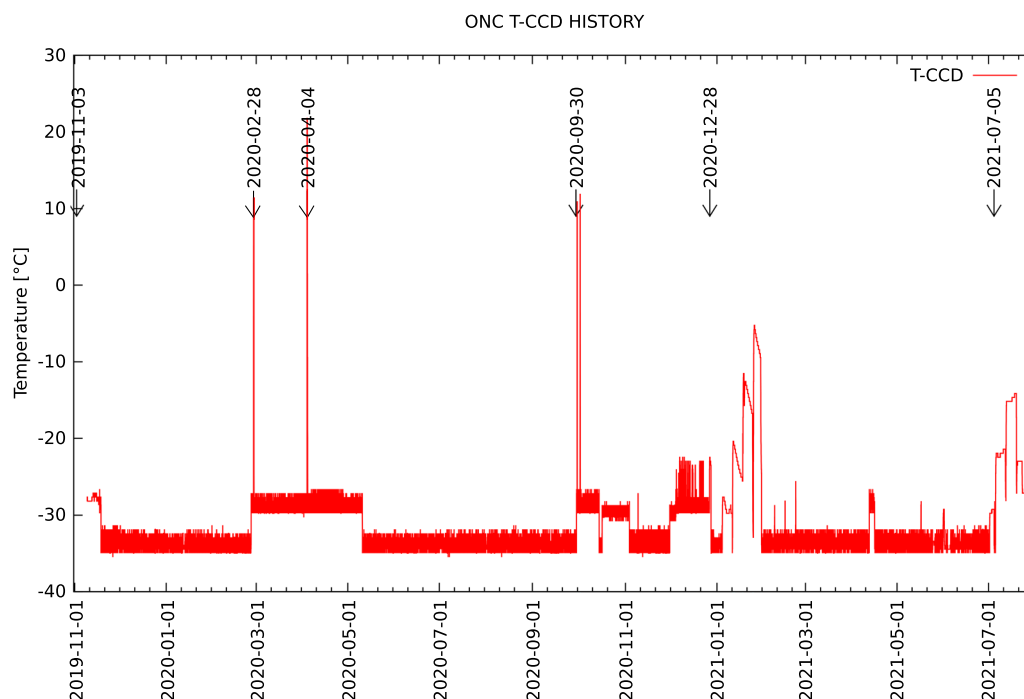


Fig. 5 History of the CCD sensor temperature for ONC-T from November 2019 to July 2021

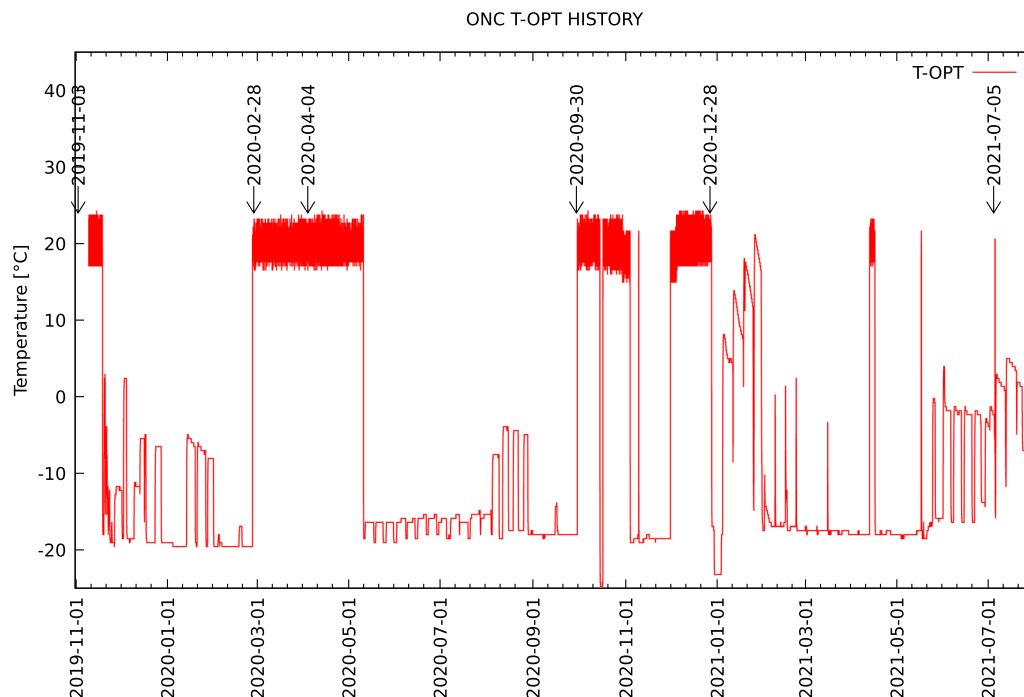


Fig. 6 Optics temperature history for ONC-T from November 2019 to July 2021

after the Earth departure until July 2021. Even if similar dark areas appear again, they will likely be eliminated by warming up the optical system and will not interfere with future observations.

Sensitivity variations of ONC-T bands based on stellar observations

Our previous efforts focused on evaluating the absolute sensitivities of ONC-T bands (Tatsumi et al. 2019) and variations in the color sensitivities relative to the *v* band ($0.55\ \mu\text{m}$) (Kouyama et al. 2021) based on stellar observations. In line with this work, we have added more stellar observations to monitor the sensitivities of ONC-T bands (Fig. 7) after the capsule re-entry operation on December 5, 2020. The list of stellar observations is summarized in Table 2. As reported in Kouyama et al. (2021), a 15% degradation in absolute sensitivity had been confirmed in the stellar observations after departure by comparing them to the sensitivity before arrival. On the other hand, only a small variation (up to 2%) in the *v*-band normalized sensitivity (i.e., sensitivity for the color ratio) was confirmed for any band during the TD operations of Hayabusa2, and the stability of the color ratio had been confirmed in the period during the return phase.

These trends were also confirmed from observations of β Sco and σ Sgr, both of which were observed before TD1 and after departure from Ryugu (Fig. 8). In them, we can ignore the uncertainty in the reference spectra used for

measuring sensitivity degradation by comparing observations of the same stellar brightness over different days. For the *ul*, *b*, and *v* bands, the degradation was stable and evaluated to be $15.8 \pm 0.4\%$, $15.3 \pm 0.3\%$, and $15.8 \pm 0.3\%$, respectively. The error ranges were evaluated from standard deviations of measured sensitivity degradations in Fig. 8. For the bands at longer wavelengths, the degradation was also 15–16%, but there were greater fluctuations (approx. 1.5% for *Na*, *w*, and *x*, and 4% for *p*) in the measurements. We could only obtain calibration observations for ϵ Aqr before and after TD1, and we could only evaluate the effect of TD1 using this star. However, the observation that the sensitivities of all seven bands are similar to each other is also found in the pre-TD1/post-TD1 comparison. Careful monitoring for possible sensitivity variations in those bands should be required in future work.

It should be noted that after the TD2 operation, the measured sensitivities from stellar observations showed a gradual decreasing trend corresponding to 2.5% per 100 days, which continued after departure from Ryugu. Kouyama et al. (2021) concluded that it was difficult to judge whether the degradation trend converged because of the insufficient number of stellar observations. With added stellar observations, however, we can conclude that the sensitivity degradation in ONC-T likely reached the convergence state for all bands in May 2020, which was before the capsule re-entry operation. The magnitude

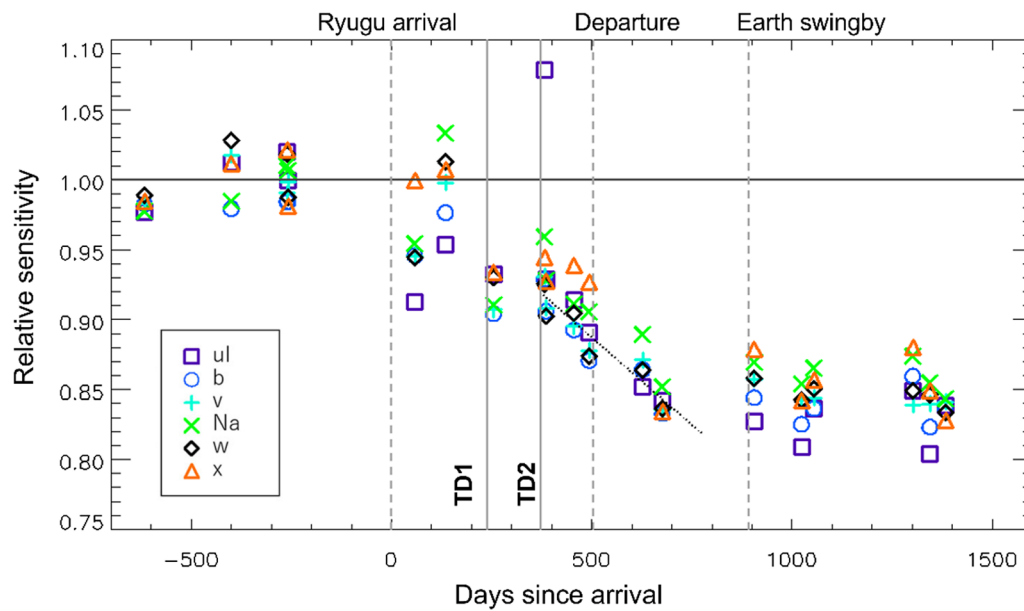


Fig. 7 Sensitivity variations of the ul–x bands measured from stellar observations since Hayabusa2’s launch. The measured sensitivity for each band was normalized by the value in Tatsumi et al. (2019), which was measured in space before arrival. A fitted trend for the sensitivity degradation of the v band after TD2 is also plotted (dotted line)

Table 2 List of stars used in Fig. 7

Observation date	Star name	HR no	V mag	Spectral type	Filters	Reference spectra
2016-10-19	ζ Peg	8634	3.40	B8V	ul, b, v, Na, w, x, p	Hamuy et al. (1992, 1994)
2017-05-23	θ Crt	4468	4.70	B9.5Vn	ul, b, v, Na, w, x, p	Hamuy et al. (1992, 1994)
2017-10-10	ε Aqr	7950	3.77	A1V	ul, b, v, Na, w, x, p	Hamuy et al. (1992, 1994)
2017-10-12	σ Sgr	7172	2.02	B2.5V	ul, b, v, Na, w, x, p	Alekseeva et al. (1996)
Arrival (2018-06-27)						
2018-08-25	β Vir	4540	3.60	F9V	ul, b, v, Na, w, x, p	Alekseeva et al. (1996)
2018-11-09	β Sco	5984	2.62	B1V	ul, b, v, Na, w, x, p	Alekseeva et al. (1996)
TD1 (2019-02-21)						
2019-03-09	ε Aqr	7950	3.77	A1V	ul, b, v, Na, w, x, p	Hamuy et al. (1992, 1994)
TD2 (2019-07-11)						
2019-07-14	ι Aur	1577	2.69	K3II	ul, b, v, Na, w, x, p	Alekseeva et al. (1996)
2019-07-18	β Tau	1791	1.65	B7III	ul, b, v, Na, w, x, p	Alekseeva et al. (1996)
2019-09-26	η Leo	3975	3.45	A0Ib	ul, b, v, Na, w, x, p	Alekseeva et al. (1996)
2019-11-03	γ Crv	4662	2.56	B8III	ul, b, v, Na, w, x, p	Alekseeva et al. (1996)
Departure (2019-11-13)						
2020-03-15	τ Sco	6165	2.82	B0.2V	ul, b, v, Na, w	Alekseeva et al. (1996)
2020-05-04	σ Sgr	7172	2.02	B2.5V	ul, b, v, Na, w, x, p	Alekseeva et al. (1996)
Capsule re-entry operation (2020-12-05)						
2020-12-19	κ Ori	2004	2.06	B0.5Ia	ul, b, v, Na, w, x, p	Alekseeva et al. (1996)
2021-04-16	β Sco	5984	2.62	B1V	ul, b, v, Na, w, x, p	Alekseeva et al. (1996)
2021-05-17	σ Sgr	7172	2.02	B2.5V	ul, b, v, Na, w, x, p	Alekseeva et al. (1996)
2022-01-19	β Vir	4540	3.60	F9V	ul, b, v, Na, w, x, p	Alekseeva et al. (1996)
2022-03-03	β Sco	5984	2.62	B1V	ul, b, v, Na, w, x, p	Alekseeva et al. (1996)
2022-04-11	σ Sgr	7172	2.02	B2.5V	ul, b, v, Na, w, x, p	Alekseeva et al. (1996)

Note that ε Aqr, β Sco, and σ Sgr were observed two times, three times, and four times, respectively

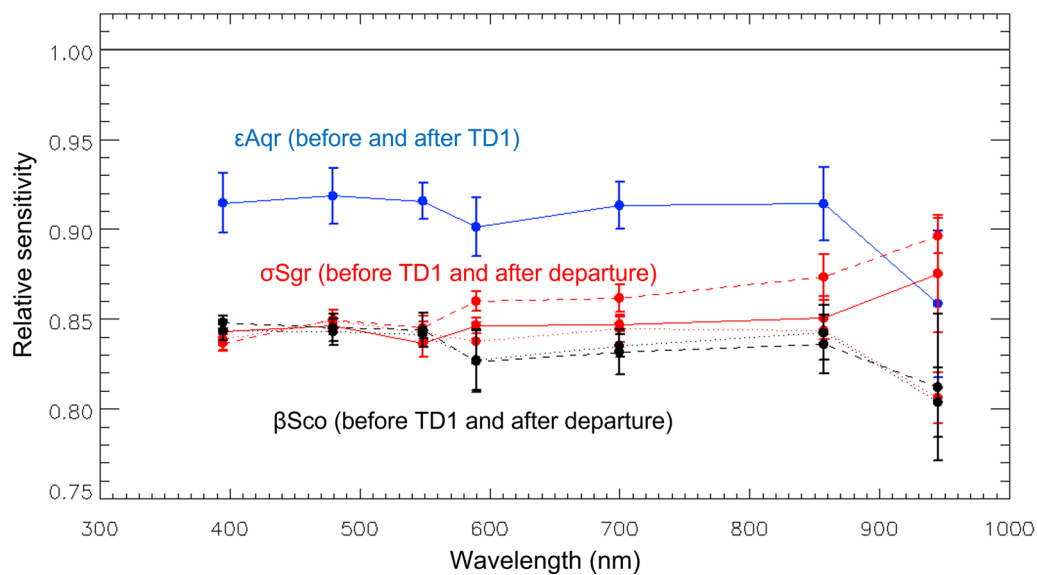


Fig. 8 Sensitivity variations of the ONC-T bands measured from specific stars that were observed more than two times

Table 3 Sensitivity factors at the reference temperature ($T_{\text{CCD}, T} = -30^\circ\text{C}$), and errors for the band ratios from stellar observations

Sensitivity (DN/s)/(W/m ² /μm/sr) at $T_{\text{CCD}, T} = -30^\circ\text{C}$								
	Filters	ul	b	v	Na	w	x	P
Before TD1 ^a	Sensitivity	439.1 ± 2.2	969 ± 7.9	1175.0 ± 10.0	546.9 ± 2.0	1515.0 ± 19.3	1499.8 ± 24.6	961.2 ± 28.8 ^b
After TD1	Sensitivity	410.1 ± 11.6	899.1 ± 22.2	1092.8 ± 25.5	510.9 ± 12.2	1418.9 ± 35.1	1405.8 ± 40.7	898.9 ± 39.8
After TD2	Degradation trend	− 0.000252 day ^{−1}						
	Sensitivity at TD2	399.7 ± 10.8	879.6 ± 22.1	1071.2 ± 25.0	498.3 ± 11.9	1380.5 ± 34.0	1373.5 ± 37.4	882.6 ± 38.9
After capsule re-entry	Sensitivity	363.3 ± 9.0	810.2 ± 16.1	988.5 ± 10.3	469.5 ± 6.7	1279.4 ± 21.8	1276.7 ± 38.2	806.2 ± 30.1 ^c

^a Tatsumi et al. (2019). ^bValue based on lunar observations. ^cValue from observing the same star at different times

of the degradation at the convergence state was almost 15% for all bands. The updated sensitivity correction coefficients are summarized in Table 3.

Here, one possible scenario for the degradation after TD2 and its stopping is that the long baffle of ONC-T might be a reservoir of dust particles at each touch down events, and such dust particles sticking inside of the baffle might move to the surface of the optics at a certain timing, which may cause opaque increasing. On the other hand, assuming that condition of dust sticking was unstable at right after touch down, while it became more stable, it might explain the stopping of the degradation trend.

However, we have to say the reasons why the gradual degradation trend happened after touch down events and why it stopped have been highly uncertain because of difficulty of monitoring physical state of the optics of ONC-T. At least, we can say that ONC-T sensitivity had been under a highly unstable condition after touch down events. The unstable condition after the second

touchdown was confirmed not only from star observations, but also from Ryugu observations (see Fig. 3.5 in Kouyama et al. 2021), which proved the stable condition of ONC-T before the first touchdown accurately. Simulation of motion of dust particles based on returned samples and reproductive experiment of inside environment of the baffle should help to understand more precise condition of ONC-T in future works.

Sensitivity variations of ONC-T bands based on lunar observations

Figures 9 and 10 show observed lunar irradiance by ONC-T bands at 08:05 a.m. on December 6, 2020 and modeled irradiance estimated from a lunar reflectance model based on SELENE/SP observations (SP model) (Yokota et al. 2011). Similar to the lunar observations in 2015 (Suzuki et al. 2018), the band ratios between the observations and the model are well-consistent, within 5%.

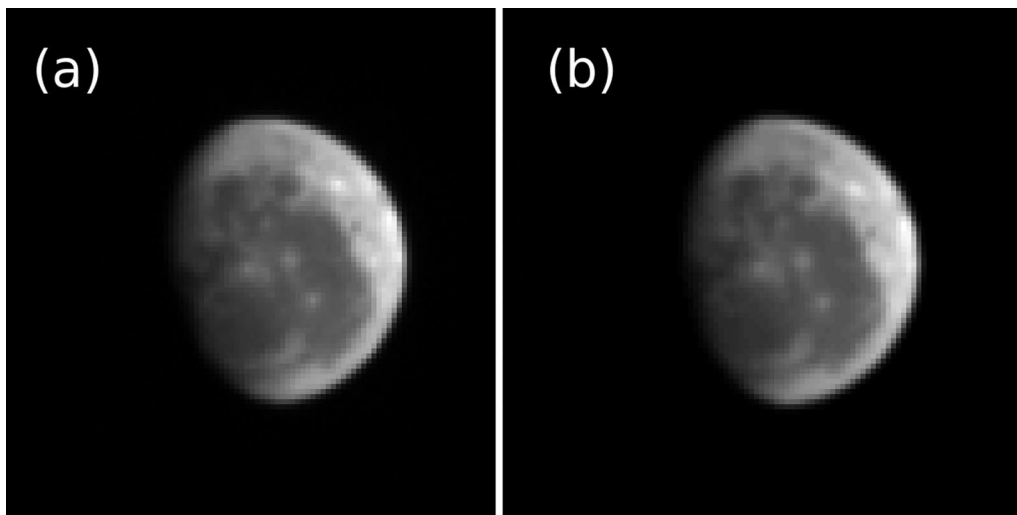


Fig. 9 **a** Lunar image obtained by ONC-T (v band) on December 6, 2020 and **b** simulated image calculated by the SP model (Yokota et al. 2011)

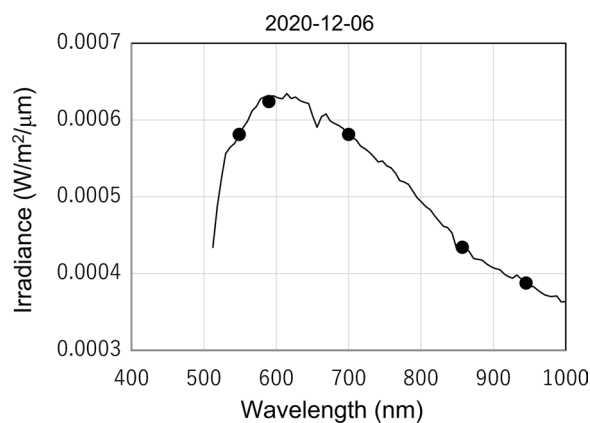


Fig. 10 Observed lunar irradiance taken at 2020-12-06 08:05 (dots) and the modeled spectrum (solid line)

Since the brightness of the Moon has been well-studied and modeled (cf. Kieffer and Stone 2005; Kouyama et al. 2016), the sensitivity of a sensor can be evaluated through a comparison between observed and modeled Moon brightness, which is called a lunar calibration. While the uncertainty in absolute accuracy from the lunar calibration is still under discussion (larger than 5%), the uncertainty for evaluating the relative variation in sensor sensitivity between different wavelength bands is sufficiently small (less than 1%), although strict geometrical conditions are required for achieving the high accuracy, such as the same phase angle condition among observations (cf. Lachérade et al. 2013; Sato et al. 2014). The observation geometries by ONC-T are summarized in Table 4.

In Fig. 11a, the ratios of observed and modeled lunar brightness in 2015 and 2020 are plotted for the v, Na, w,

Table 4 Moon observation geometries

Date	2015-12-05	2020-12-06
Distance (km)	764,495	572,053
Phase angle	59.3°	49.4°
Sub spacecraft longitude	− 96.2°	− 26.0°
Sub spacecraft latitude	− 56.4°	8.0°

x, and p bands. Compared to the results from 2015, those from 2020 indicate clear sensitivity degradation in all bands.

Figure 11b shows quantitative evaluations of the sensitivity degradation between 2015 and 2020. The results indicate a 10% degradation for all bands. The 10% degradation from the lunar calibration is somewhat smaller than degradation estimations from the stellar and Ryugu observations (approx. 15%; Fig. 8) (Kouyama et al. 2021). This approximately 5% discrepancy in sensitivity degradation can be considered from uncertainty of the lunar calibration due to rather large difference between observation phase angles in 2015 and 2020 (10° difference at a high phase angle condition). Therefore, we consider the result from lunar calibration as a reference for confirming significant sensitivity degradation in this study. We expect more quantitative evaluation from lunar calibration by additional Moon observations at future Earth swing-by.

Low stray light attitude and noise evaluation in extended missions

To expand the range of possible targets for ONC-T observations, such as to zodiacal light observations and

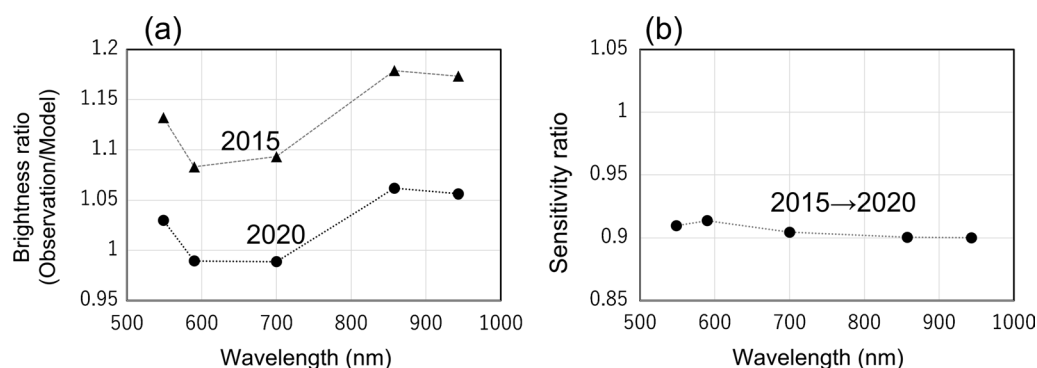


Fig. 11 **a** Ratios between the observed and modeled lunar brightness. The model brightness was estimated based on the SP model. **b** Sensitivity degradation between 2015 and 2020 for the lunar observations evaluated in (a)

observations of transiting exoplanets, before arrival at the next asteroid in the extended mission, a method for reducing stray light was investigated. It was reported in Suzuki et al. (2018) and Tatsumi et al. (2019) that sunlight reaches the CCD through a small gap near the ONC-T radiator when the spacecraft is oriented in attitudes that allow sunlight to be incident on it. The ONC radiator is mounted on the $-Y$ panel of the spacecraft and is also close to the $+X$ side. Therefore, if the spacecraft is oriented, so that the Sun shines on the $-X$ and $+Y$ sides of the spacecraft, then sunlight will not shine directly on the radiator.

Until the capsule was released to Earth in December 2020, the spacecraft was operated in such a way that the $-X$ side of it was not exposed to sunlight. This was done to protect the capsule, which was placed on that side. This restriction was removed after capsule separation. The “stray light from the ONC-T radiator” should be reduced by keeping the Sun on the $-X$ and $+Y$ sides of the spacecraft.

Figure 12 shows the ONC-T stray light intensity ($\log[\text{DN/s}]$, where DN is the digital number) for the spacecraft attitude from the arrival in June 2018 to departure in December 2020, using the same method as Tatsumi et al. (2019). Observations indicated by the gray circles were taken with long exposures of 100 s or more. The amount of stray light is small in the region where sunlight is incident on the spacecraft’s $-X$ panel ($\text{XPNL} < 0$) and $+Y$ panel ($\text{YPNL} > 0$). Depending on the spacecraft attitude, relatively high stray light (~ 1000 DN/s) may enter image in the worst cases, but it can be reduced by a factor of 100 by setting the spacecraft to appropriate attitude.

After capsule separation on December 5, 2020, we attempted observations with long exposures of more than 100 s with the Sun on the $-X$ side of the spacecraft, and we confirmed that the signal due to stray light or noise was

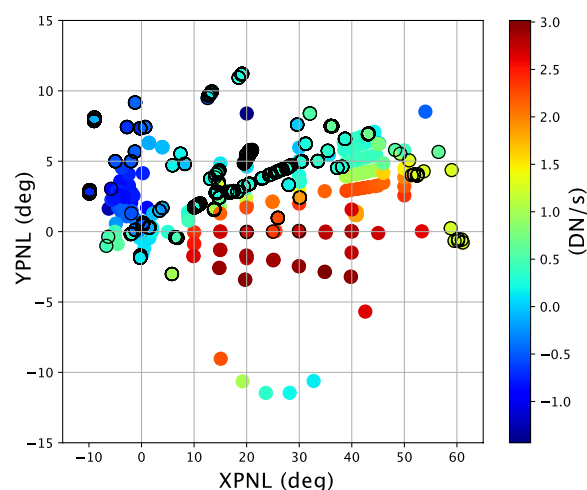


Fig. 12 Stray light intensity ($\log[\text{DN/s}]$) of ONC-T for spacecraft attitudes taken from June 27, 2019 to December 26, 2020. Black circles show observations made with a long exposure (> 100 s). XPNL and YPNL represent the solar incidence angle on the spacecraft’s X and Y panel, respectively

less than 0.2 DN/s. According to Kameda et al. (2017), the dark current noise of ONC-T at a CCD temperature of -20°C is approximately 0.1 DN/s, and the < 0.2 DN/s result obtained in this trial is comparable to this value. The maximum exposure time of the ONC-T is about 178 s, and even for a target with a very small signal, if 36 counts or more can be expected in that time, then it is possible to image with a signal-to-noise ratio of 1 or better.

Prediction of the sensitivity change and exposure time for the extended mission

A comparison of ONC-T sensitivity changes for the FF lamp and stellar observations shows good agreement, except that no stellar observations were made

immediately after launch. Thus, the rapid initial decrease in the *ul* band observed in the FF-lamp observation cannot be supported with stellar observation. In both observation results, no significant decrease in sensitivity occurred after the return to Earth (capsule re-entry) in December 2020.

We made simple models for predicting future changes in the sensitivity of ONC-T, whose purpose is to evaluate the feasibility of observing the asteroids 2001 CC₂₁ and 1998 KY₂₆ during the extended mission. Figure 13 shows two potential cases for the sensitivity change (Table 3) of the *v* band that are obtained from stellar observations: (1) no sensitivity decrease and, as the worst case, (2) a decrease rate of 2%/1302 days seen in the early days of FF-lamp observations. In the first case, the relative sensitivity remains 84.1% after April 15, 2020. In the other case, the relative sensitivities during the approach of asteroids 2001 CC₂₁ and 1998 KY₂₆ are estimated to be 80.6% and 77.8%, respectively.

The brightness and albedo of asteroids 2001 CC₂₁ (Binzel et al. 2004) and 1998 KY₂₆ (Ostro et al. 1999) have been reported, but the albedo values of them are highly uncertain at this time. Here, we consider a range of albedo values for the target asteroids with a lower limit of 4%, the same as Ryugu, and an upper limit of 20%.

The brightness of asteroids 2001 CC₂₁ and 1998 KY₂₆ was compared to that of Ryugu, taking into account the distance between the asteroids and the Sun. This brightness ratio is, in other words, the ratio of the exposure time required to image Ryugu with ONC-T to the exposure time required to image the asteroids 2001 CC₂₁ and 1998 KY₂₆ (Table 5). 2001 CC₂₁ requires a shorter exposure time than Ryugu due to its smaller solar distance, while 1998 KY₂₆ requires a longer exposure time owing to its larger solar distance. Exposure times for imaging Ryugu ranged from 65 to 131 ms in the *v* band. The range of exposure time for Ryugu was narrow, because the positional relationship between the solar panel fixed to the spacecraft and the camera viewing direction was a constraining condition, resulting in a limited range of phase angle imaging. By multiplying this range of exposure times by the exposure time ratios in Table 5, we can estimate that asteroid 2001 CC₂₁ can be imaged with exposure times ranging from 11 to 110 ms, and asteroid 1998 KY₂₆ with exposure times ranging from 22 to 219 ms. These ranges are within the range of the possible ONC-T exposure time settings. These exposure times are the time required to obtain a signal of approximately 2000 DN of the asteroid. Thus, the predicted signal rate at 2001 CC₂₁ and 1998 KY₂₆ are 18,000–1800 DN/s and

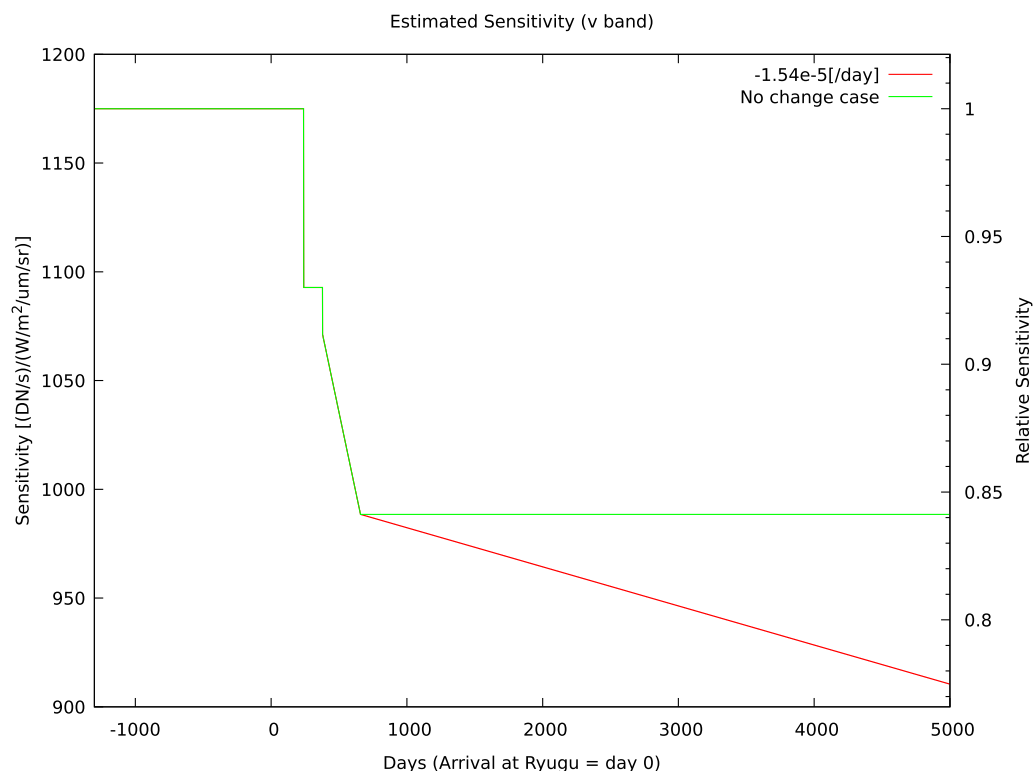


Fig. 13 Model of sensitivity changes for ONC-T in the *v* band. Changes up to April 15, 2020 are from stellar observations (Table 3). After that, the red line shows the case with a sensitivity decrease, and the green line shows the case with no change

Table 5 Estimated relative sensitivities and exposure time ratios for the new target asteroids

Asteroid	Ryugu	2001 CC ₂₁	1998 KY ₂₆
Spectral types	C	L	L
Arrival date*	2018/06/27	2026/07/15	2031/07/15
Days since arrival at Ryugu	0	2940	4766
Estimated relative sensitivity [%]	–	80.6–84.1	77.8–84.1
Heliocentric distance [km]	1.4665E + 08	1.2062E + 08	1.6710E + 08
Albedo [%]	4	20	20
Exposure time ratio**	1	0.17	0.33

*Because the exact arrival date has not yet been determined, we chose a date near the middle of the expected arrival month

**Value for the worst expected sensitivity

90,000–9000 DN/s, respectively. These signal rates are large even when compared to the signal rate of stray light in the worst case (1000 DN/s). With the exception of the wide band, all bands were within the settable exposure time range, and it was confirmed that ONC-T could observe asteroids 2001 CC₂₁ and 1998 KY₂₆. The wide band used for Ryugu imaging had an exposure time of 8 ms, two steps higher than the minimum setting (0 s), so the exposure time could not be set sufficiently short to cope with the high albedo of 2001 CC₂₁, indicating that the signal would saturate. If the exposure time setting is increased by one step, the exposure time is approximately multiplied by the square root of two.

ONC-W1 and W2 sensitivities since departure from Ryugu

The ONC onboard Hayabusa2 has two wide-angle cameras, W1 (nadir view) and W2 (oblique view) (Suzuki et al. 2018). These cameras do not have FF lamps or high enough sensitivities to observe most stars, so we did not have a chance to perform a quantitative health check after the departure from Ryugu. Thus, the Earth return was one of the few opportunities to examine the health of W1 and W2. Furthermore, since the spacecraft reached very close to Earth (approx. 300 km from the surface) when the capsule re-entered the atmosphere, this provided a unique opportunity for observing a fast-moving object relative to the spacecraft. In this section, we discuss the results of the Earth observations and infer the health conditions of the cameras.

Status of ONC-W1

Earth imaging using ONC-W1 was successfully performed during the return to Earth in December 2020. The exposure time used was 8.2 ms, which is the same as that used in 2015. Photometric differences are not taken into account, because the small visual diameter in the 2015 Earth image only allows comparison of the dark

areas of the ocean that were confirmed to be cloud-free. While the counts of the oceans in 2015 were about 500 to 600, those in 2020 were about 300 to 400. Assuming that this difference in brightness (approx. 60%) is due to the sensitivity degradation, it is comparable to that reported in Kouyama et al. (2021).

ONC-W1 was designed to capture Ryugu images with approximately the same exposure time as the ONC-T. On the other hand, ONC-W1 was also designed to enable target marker imaging using the flash lamp during TD, which was expected to be much brighter than Ryugu. To cover both requirements, ONC-W1 has shorter minimum (170 μ s) and maximum (5.6 s) exposure times than those for ONC-T. If ONC-W1 had no sensitivity degradation, then stars brighter than magnitude 1.2 could be observed with the maximum exposure time. However, because of the limited exposure duration and the significant sensitivity degradation of ONC-W1, observations of Formalhaut (visual magnitude of 1.2) in May 2022 produced no stellar image.

On the other hand, Jupiter observations in April 2020, which was brighter than a visual magnitude of 0, produced a bright image of Jupiter that was clearly confirmed in the W1 image. Since ONC-W1 conducted Jupiter observations in February 2016 in the cruising phase to Ryugu, meaning before sensitivity degradation, it is possible to measure the sensitivity degradation by comparing observed brightness of Jupiter. By applying correction of observation geometries in 2016 and 2020 following Tatsumi et al. (2019), which enables to compare two observations with different distance and phase angle conditions, we confirmed that the magnitude of sensitivity degradation in ONC-W1 was $61 \pm 3\%$. This result is highly consistent with the measured sensitivity degradation in Kouyama et al. (2021). The sensitivity of ONC-W1 should be monitored periodically until the arrival of the target asteroid in the future using opportunities when brighter stars and Jupiter are observable and when the spacecraft performs another flyby of Earth.

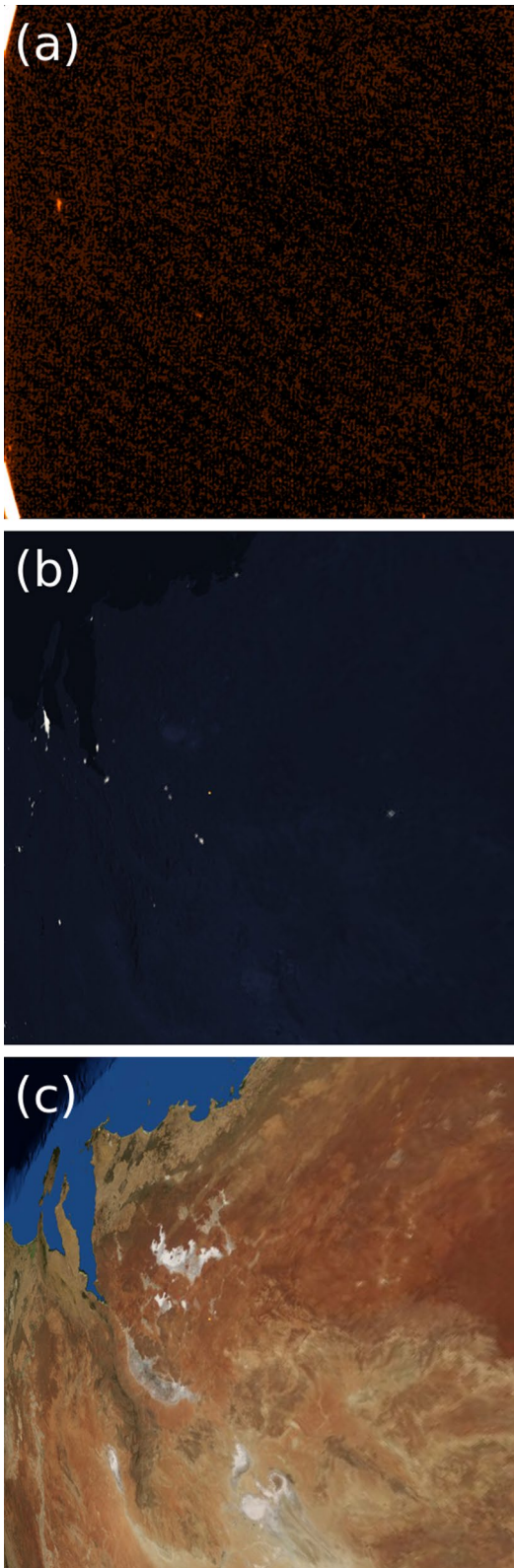


Fig. 14 **a** Australia imaged by ONC-W2 at 02:29 a.m. on December 6, 2020 (2 min before closest approach to Earth). The bright spot on the left of the image comes from the city lights of Adelaide. **b** Simulated night view of an ONC-W2 image at the same time. **c** Simulated image with the topography visible

Status of ONC-W2

ONC-W2 was designed to image Ryugu with about 1/6 the exposure time of ONC-T. The maximum exposure time for ONC-W2 was 45 s. If ONC-W2 had no sensitivity degradation, then stars brighter than magnitude 4.6 could be observed with the maximum exposure time. During the return phase, ONC-W2 observed Vega (magnitude 0.03) with the maximum exposure time on February 28, 2020. Vega was successfully captured with sufficient DN, that is, approx. 1100 DN, or a signal-to-noise [S/N] ratio of 200 if we consider only background noise level. Even if hot-pixel existence is considered, the measurement still achieved 30–40 S/N ratio. From the observation, the observed Vega brightness was $86 \pm 4\%$ of expected brightness for which we assume that no-degradation happens on ONC-W2, that is, ONC-W2 has the sensitivity of 3.8×10^3 (DN/s)/(W/m²/sr/μm) (Tatsumi et al. 2019).

It should be noted that Vega position in the ONC-W2 field of view (FOV) was far from center, and it was hard to quantitatively evaluate its sensitivity variation due to uncertainty in the flat field correction for such a region (up to 15%, Tatsumi et al. 2019). Although it is difficult to provide a quantitative conclusion for ONC-W2 sensitivity due to the large uncertainty in flat field correction for stars, at least, we can say ONC-W2 did not experience significant sensitivity degradation that ONC-W1 experienced (~60% degradation), and this should be due to difference of W2's boresight direction from W1's direction.

The boresight direction of ONC-W2 is tilted approximately 60 degrees from that of ONC-T. The unique installation angle of this camera was used to attempt imaging of Earth and the capsule during the Earth swing-by on December 6, 2020. Continuous imaging with 1-s exposures was performed, but the capsule could not be detected (see [Appendix](#) for details). On the other hand, it successfully observed the city lights of Adelaide and cloud-like patterns over Australia (Fig. 14). These results indicate that W2 is still functional and has not experienced severe deterioration in sensitivity.

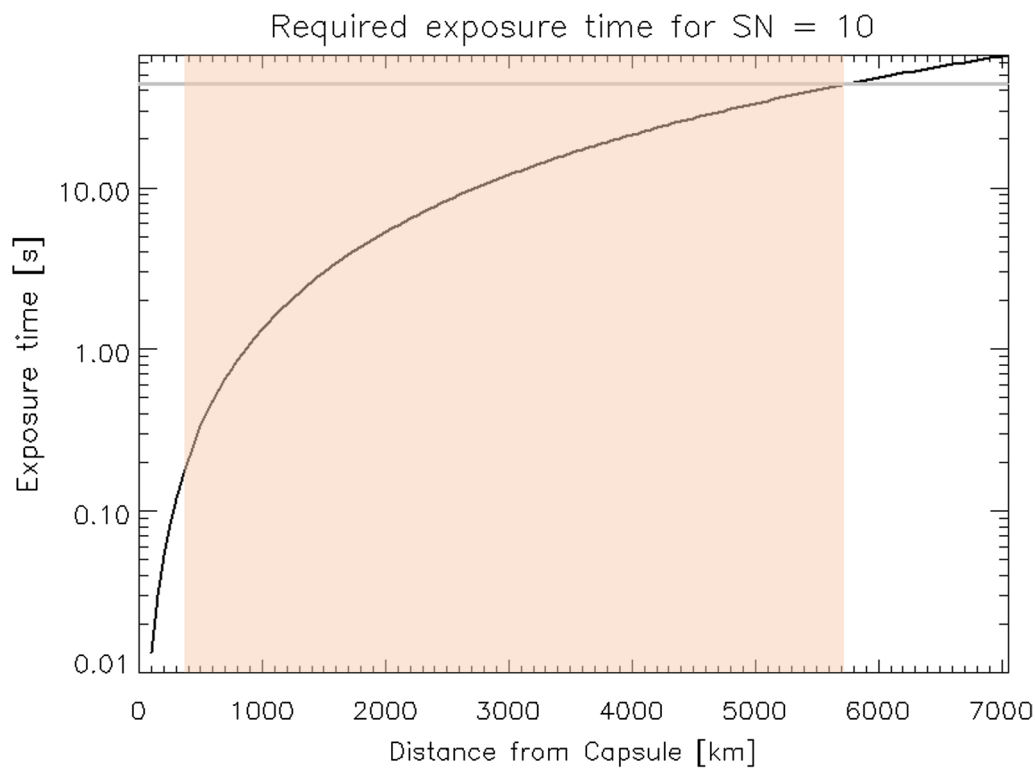


Fig. 15 Required exposure times for observing the return capsule with a S/N ratio of 10 as a function of observation distance. A gray line indicates the maximum exposure time of ONC-W2 (44 s), and the orange colored region indicates conditions in which ONC-W2 is capable of observing the capsule

Conclusion

The star observation data, which is the most reliable among our calibration sources, obtained after departure from asteroid Ryugu suggest that ONC-T optical sensitivity degradation may have settled down by 400–500 days after the first touchdown (i.e., ~700th day after Ryugu arrival) and that the subsequent change in sensitivity is within the error of stellar calibrations. Based on the FF-lamp measurement data, which gives worse trend than the star observation data, we obtained lower estimates for transmission during the extended mission. Assuming that the rate of change in sensitivity seen on the FF-lamp before Ryugu arrival continues after 700th day, the ONC-T sensitivity is estimated to be between 80.6% and 84.1% during the 2001 CC₂₁ flyby and 77.8% and 84.1% during the 1998 KY₂₆ flyby, respectively. Thus, even if this pessimistic linear decrease trend after 700th day is real, it will not pose a serious problem for asteroid observations in the extended mission. These sensitivity levels are expected to be sufficient for performing the necessary observations of these asteroids. Although the extended mission period is long, calibration should be repeated throughout the extended mission to track changes in sensitivity.

During the cruise preceding Hayabusa2's arrival at the target asteroids in the extended mission, opportunities for ecliptic light observations and exoplanet observations can be increased by reducing noise from attitudes in which the Sun shines on the $-X$ and $+Y$ panels of the spacecraft.

Appendix

Observation with ONC-W2 during the re-entry phase of the return capsule

See Figs. 15, 16, 17, 18 and 19

Since ONC-W2 was rarely used during the return cruise, even during the proximity phase after TD2, it has not been confirmed that any significant optical degradation occurred. We attempted to use the unique installation angle of this camera to image Earth and the capsule during the Earth swing-by operation. We decided to include it in this study as part of a qualitative optical degradation assessment.

Based on the observational result of the maximum brightness of Hayabusa's return capsule during the re-entry phase of its 2010 mission, the maximum temperature of the return capsule was expected to be around

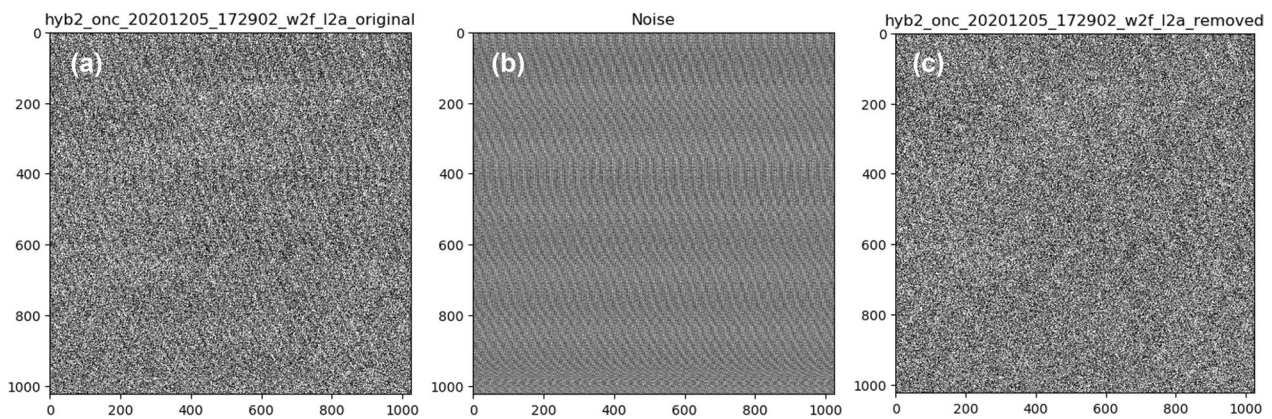


Fig. 16 **a** Example of an ONC-W2 image when the capsule is expected to have maximum thermal emission. **b** Synthetic image generated from the top-10 Fourier components in **(a)**. **c** Noise reduced image derived from **(a, b)**

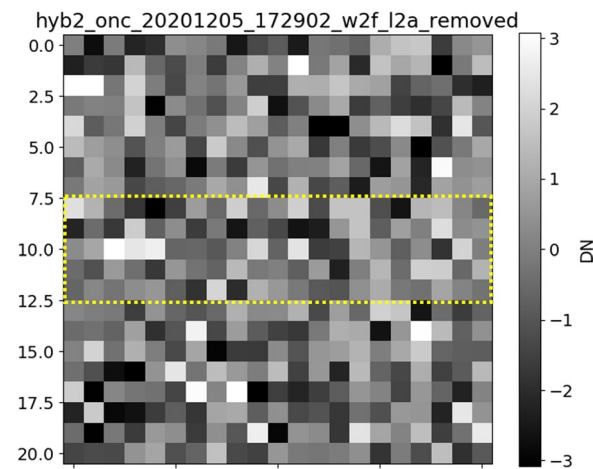


Fig. 17 Close-up of an ONC-W2 image that includes the expected region where the return capsule was observed (indicated by a dotted rectangle), taken at 17:29:02 p.m. on December 5, 2022

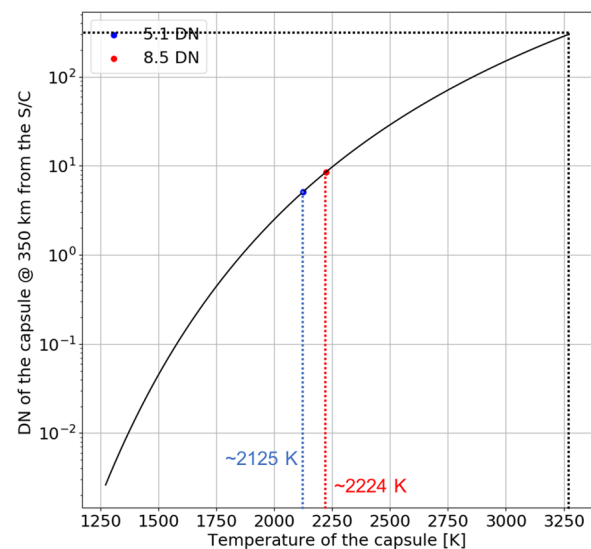


Fig. 18 Relationship between the apparent brightness temperature and the DNs of ONC-W2, observed from a 350 km distance

3000 °C from considerations of blackbody emission, and the altitude during maximum brightness was 55–60 km (Sato et al. 2012). We assumed that the return capsule of Hayabusa2 would also reach maximum brightness temperature at 55–60 km. The estimated distance between the capsule and the Hayabusa2 spacecraft would be around 350–400 km at the time of maximum brightness.

Although the size of the capsule (40 cm diameter) was much smaller than the corresponding spatial scale of a ONC-W2 pixel (400 m), even from the minimum distance of 350 km, we confirmed that the capsule would be bright enough to be observed (i.e., the S/N ratio would be 10) within the possible exposure times, assuming a 3000 °C capsule temperature (Fig. 15). If W2 observes the capsule from a distance of 350 km, then 1 s of exposure

would be enough for unambiguous detection if the object were moving with respect to Hayabusa2.

However, it was also expected that the motion of the capsule in the W2 FOV would be approximately 10 pixels within the 1-s exposure owing to the velocity difference between Hayabusa2 and the capsule. Therefore, an effective exposure time for the capsule observation would be 0.1 s, and the possible S/N ratio would be around 5. Although the expected S/N ratio could be marginal, we conducted observations using 1-s exposures with an interval of 2 s during the re-entry phase of the return capsule.

Figure 16a shows an example of the images obtained on December 5, 2020 during this phase. Since there were clear periodic noise patterns (due to electromagnetic noise),

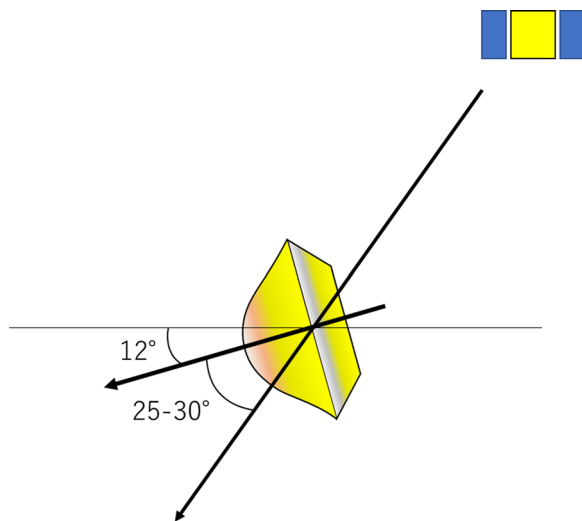


Fig. 19 Schematic view of the capsule observation geometry for ONC-W2 at the time of maximum brightness, based on the planned trajectory information for the capsule and Hayabusa2

we performed Fourier analysis for each image (Fig. 16b) and reduced the noise by subtracting the top-10 Fourier components for each line, thus enhancing their visibility (Fig. 16c). The formula for doing this can be given by

$$g_i(x) = \sum_{j=1}^{10} a_j \sin(2\pi f_j x - b_j),$$

where a_j indicates the amplitude of the j th largest Fourier component, and b_j and f_j are its phase and wavenumber, respectively.

Figure 17 shows a close-up image that includes the region where the capsule was expected to be observed. In this region, there was no clear bright spot that exceeded a S/N level of 3 or 5, compared with the surrounding region. The standard deviation of counts in the image was 1.7 DN; the S/N levels of 3 and 5 corresponded to 5.1 DN and 8.5 DN, respectively.

It is difficult to discuss the implications of an observation result in which no significant signal was detected. However, the unique nature of this particular observation allows us to infer the significance of the fact that ONC-W2 did not detect light from the aerodynamically heated side of the capsule. From the sensitivity and spectral response performance of ONC-W2 (Suzuki et al. 2018; Kouyama et al. 2021), the brightness temperatures that provide 5.1 DN and 8.5 DN for ONC-W2 from a 350 km distance are 2125 and 2224K, respectively (Fig. 18). This means that the apparent brightness temperature from ONC-W2 might not reach 3000 °C.

It should be noted from the investigation of the return capsule of the first mission that the back side of the

capsule experienced only approximately 650K heating (Sato et al. 2012), while the front side of the capsule experienced 3000 °C. Therefore, if ONC-W2 observed both the front and back sides of the capsule, then the apparent brightness of it should be much darker than the brightness for 3000 °C.

Figure 19 shows a schematic view of a geometric configuration for the capsule observation by ONC-W2 based on the planned trajectories of the capsule and Hayabusa2 during the re-entry phase. Assuming the shape of the capsule to be a sphere for simplicity, the front side of it (higher temperature) occupies only 6.7% of the capsule's silhouette seen from ONC-W2. In this case, the apparent brightness of the capsule corresponds to 2150K, even if the front side of the capsule reached 3000 °C. A temperature of 2150K is almost the same as that for a S/N level of 3, and thus, the geometric configuration and relatively low temperature of the capsule's backside can be reasons why ONC-W2 could not capture a clear signal from the capsule.

It has been noted that post-flight analysis of the onboard accelerometers indicates that the attitude of the return capsule was very stable at high altitudes, where high aerodynamic heating took place. A large-amplitude rotation only took place at low altitudes ≤ 20 km (Yamada and Yoshihara 2022). This is consistent with our result that ONC-W2 did not detect significant light during the atmospheric re-entry of the capsule.

Abbreviations

ONC:	Optical navigation camera
JAXA:	Japan Aerospace Exploration Agency
CCD:	Charge-coupled device
ONC-T:	Optical Navigation Camera Telescope
ONC-W1:	Optical Navigation Camera Telescope Wide-angle 1 (nadir view)
ONC-W2:	Optical Navigation Camera Telescope Wide-angle 2 (slant view)
FF:	Flat Field
TD:	Touchdown
TD1:	First touchdown
TD2:	Second touchdown
ONC-AE:	ONC analog electric unit
DN:	Digital number
S/N:	Signal-to-noise
FOV:	Field of view

Acknowledgements

The authors would like to thank the entire Hayabusa2 project team for their efforts in supporting our inflight calibrations in this paper. We are grateful to NEC Inc. Co., who made the flight model of the ONC. We would like to thank Dr. S. Nakazawa for his advice and supporting instruments temperature control during our calibrations.

Author contributions

MY summarized the data and wrote the manuscript with contributions from TK and SS. MY, TK, KY, ET, NT, and YY analyzed the data and prepared the figures and tables in this paper. All authors contributed to ONC data

acquisitions, reduction, and interpretation. All authors read and approved the final manuscript.

Funding

This study was supported by the Japan Society for the Promotion of Science (JSPS) Core-to-Core Program "International Network of Planetary Sciences" and KAKENHI Grant Number 20H00194.

Availability of data and materials

The data sets generated and/or analyzed during this study will be made available in the Hayabusa2 Science Data Archives on the Data Archives and Transmission System (DARTS) repository, at <https://www.darts.isas.jaxa.jp/planet/project/hayabusa2/>.

Declarations

Ethics approval and consent to participate

Not applicable.

Consent for publication

Not applicable.

Competing interests

The authors declare that they have no competing interests.

Author details

¹Planetary Exploration Research Center, Chiba Institute of Technology, Narashino, Chiba 275-0016, Japan. ²Digital Architecture Research Center, National Institute of Advanced Industrial Science and Technology, 2-3-26, Aomi, Koto-ku, Tokyo 135-0064, Japan. ³Department of Earth and Planetary Science, University of Tokyo, Bunkyo-ku, Tokyo 113-0033, Japan. ⁴Instituto de Astrofísica de Canarias (IAC), University of La Laguna, 38205 Tenerife, Spain. ⁵Institute of Space and Astronautical Science, Japan Aerospace Exploration Agency, Sagami-hara, Kanagawa 252-5210, Japan. ⁶Geological Survey of Japan, National Institute of Advanced Industrial Science and Technology, Tsukuba, Ibaraki 305-8567, Japan. ⁷Center for Data Science, Ehime University, Matsuyama, Ehime 790-8577, Japan. ⁸University of Aizu, Aizu-Wakamatsu, Fukushima 965-8580, Japan. ⁹Rikkyo University, 3-34-1 Nishi-Ikebukuro, Toshima, Tokyo 171-8501, Japan. ¹⁰Meiji University, Kawasaki, Kanagawa 214-8571, Japan. ¹¹Department of Complexity Science and Engineering, University of Tokyo, Kashiwa, Chiba 277-8561, Japan. ¹²JAXA Space Exploration Center, Japan Aerospace Exploration Agency (JAXA), Sagami-hara, Kanagawa 252-5210, Japan. ¹³Kobe University, Kobe, Hyogo 657-8501, Japan.

Received: 29 July 2022 Accepted: 18 February 2023

Published online: 13 March 2023

References

- Alekseeva GA, Arkharov AA, Galkin VD, Hagen-Thorn EI, Nikanorova IN, Novikov VV, Novopashenny VB, Pakhomov VP, Ruban EV, Shchegolev DE (1996) The Pulkovo spectrophotometric catalog of bright stars in the range from 320 to 1080 nm. *Balt Astron* 5:603–838
- Arakawa M, Saiki T, Wada K, Ogawa K, Kadono T, Shirai K, Sawada H, Ishibashi K, Honda R, Sakatani N, Iijima Y, Okamoto C, Yano H, Takagi Y, Hayakawa M, Michel P, Jutzi M, Shimaki Y, Kimura S, Mimasu Y, Toda T, Imamura H, Nakazawa S, Hayakawa H, Sugita S, Morota T, Kameda S, Tatsumi E, Cho Y, Yoshioka K, Yokota Y, Matsuoka M, Yamada M, Kouyama T, Honda C, Tsuda Y, Watanabe S, Yoshikawa M, Tanaka S, Terui F, Kikuchi S, Yamaguchi T, Ogawa N, Ono G, Yoshikawa K, Takahashi T, Takei Y, Fujii A, Takeuchi H, Yamamoto Y, Okada T, Hirose C, Hosoda S, Mori O, Shimada T, Soldini S, Tsukizaki R, Iwata T, Ozaki M, Abe M, Namiki N, Kitazato K, Tachibana S, Ikeda H, Hirata N, Hirata N, Noguchi R, Miura A (2020) An artificial impact on the asteroid (162173) Ryugu formed a crater in the gravity-dominated regime. *Science* 368:67–71. <https://doi.org/10.1126/science.aaz1701>
- Binzel RP, Perozzi E, Rivkin AS, Rossi A, Harris AW, Bus SJ, Valsecchi GB, Slivan SM (2004) Dynamical and compositional assessment of near-Earth object mission targets. *Meteorit Planet Sci* 39:351–366
- Hamuy M, Walker AR, Suntzeff NB, Gigoux P, Heathcote SR, Phillips MM (1992) Southern Spectrophotometric Standards, vol. 104, no. 677. Astronomical Society of the Pacific, Publications, pp 533–552 (ISSN 0004-6280).
- Hamuy M, Suntzeff NB, Heathcote SR, Walker AR, Gigoux P, Phillips MM (1994) Southern Spectrophotometric Standards, 2. vol. 106, no. 700. Astronomical Society of the Pacific, Publications, pp 566–589 (ISSN 0004-6280).
- Hirabayashi M, Mimasu Y, Sakatani N, Watanabe S, Tsuda Y, Saiki T, Kikuchi S, Kouyama T, Yoshikawa M, Tanaka S, Nakazawa S, Takei Y, Terui F, Takeuchi H, Fujii A, Iwata T, Tsumura K, Matsuoka S, Shimaki Y, Urakawa S, Ishibashi Y, Hasegawa S, Ishiguro M, Kuroda D, Okumura S, Sugita S, Okada T, Kameda S, Kamata S, Higuchi A, Senshu H, Noda H, Matsumoto K, Suetsugu R, Hirai T, Kitazato K, Farnocchia D, Naidu SP, Tholen DJ, Hergenrother CW, Whiteley RJ, Moskovitz NA, Abell PA (2021) Hayabusa2 extended mission: New voyage to rendezvous with a small asteroid rotating with a short period. *Adv Space Res* 68(3):1533–1555. <https://doi.org/10.1016/j.asr.2021.03.030>
- Honda R, Arakawa M, Shimaki Y, Shirai K, Yokota Y, Kadono T, Wada K, Ogawa K, Ishibashi K, Sakatani N, Nakazawa S, Yasui M, Morota T, Kameda S, Tatsumi E, Yamada M, Kouyama T, Cho Y, Matsuoka M, Suzuki H, Honda C, Hayakawa M, Yoshioka K, Hirata N, Hirata N, Sawada H, Sugita S, Saiki T, Imamura H, Takagi Y, Yano H, Okamoto C, Tsuda Y, Iijima Y (2021) Resurfacing processes on asteroid (162173) Ryugu caused by an artificial impact of Hayabusa2's Small Carry-on Impactor. *Icarus* 366:114530. <https://doi.org/10.1016/j.icarus.2021.114530>
- Kameda S, Suzuki H, Cho Y, Koga S, Yamada M, Nakamura T, Hiroi T, Sawada H, Honda R, Morota T, Honda C, Takei A, Takamatsu T, Okumura Y, Sato M, Yasuda T, Shibasaki K, Ikezawa S, Sugita S (2015) Detectability of hydrous minerals using ONC-T camera onboard the Hayabusa2 spacecraft. *Adv Space Res* 56(7):1519–1524. <https://doi.org/10.1016/j.asr.2015.06.037>
- Kameda S, Suzuki H, Takamatsu T, Cho Y, Yasuda T, Yamada M, Sawada H, Honda R, Morota T, Honda C, Sato M, Okumura Y, Shibasaki K, Ikezawa S, Sugita S (2017) Preflight calibration test results for Optical Navigation Camera Telescope (ONC-T) onboard the Hayabusa2 spacecraft. *Space Sci Rev* 208:17–31. <https://doi.org/10.1007/s11214-015-0227-y>
- Kieffer HH, Stone TC (2005) The Spectral Irradiance of the Moon. *Astron J* 129:2887–2901
- Kouyama T, Yokota Y, Ishihara Y, Nakamura R, Yamamoto S, Matsunaga T (2016) Development of an Application Scheme for the SELENE/SP Lunar Reflectance Model for Radiometric Calibration of Hyperspectral and Multispectral Sensors. *Planet Space Sci* 124:76–83
- Kouyama T, Tatsumi E, Yokota Y, Yumoto K, Yamada M, Honda R, Kameda S, Suzuki H, Sakatani N, Hayakawa M, Morota T, Matsuoka M, Cho Y, Honda C, Sawada H, Yoshioka K, Sugita S (2021) Post-arrival calibration of Hayabusa2's optical navigation cameras (ONCs): Severe effects from touchdown events. *Icarus* 360:114353. <https://doi.org/10.1016/j.icarus.2021.114353>
- Lachérade S, Viticchié B, Stone T, Lebégue L, Wagner S, Hewison T (2013) On the phase-angle dependence of the moon calibration results. *GSICS Q*. <https://doi.org/10.7289/V5N877QQ>
- Mimasu Y, Kikuchi S, Takei Y, Saiki T, Watanabe S, Tanaka S, Hirabayashi M, Sakatani N, Kouyama T, Yoshikawa M, Nakazawa S, Tsuda Y (2022) 27. Extended mission of Hayabusa2. In: Hirabayashi M, Tsuda Y (eds) Hayabusa2 asteroid sample return mission technological innovations and advances, 1st edn. Elsevier, Amsterdam
- Morota T, Sugita S, Cho Y, Kanamaru M, Tatsumi E, Sakatani N, Honda R, Hirata N, Kikuchi H, Yamada M, Yokota Y, Kameda S, Matsuoka M, Sawada H, Honda C, Kouyama T, Ogawa K, Suzuki H, Yoshioka K, Hayakawa M, Hirata N, Hirabayashi M, Miyamoto H, Michikami T, Hiroi T, Hemmi R, Barnouin OS, Ernst CM, Kitazato K, Nakamura T, Riu L, Senshu H, Kobayashi H, Sakaki S, Komatsu G, Tanabe N, Fujii Y, Irie T, Suemitsu M, Takaki N, Sugimoto C, Yumoto K, Ishida M, Kato H, Moroi K, Domingue D, Michel P, Pilorget C, Iwata T, Abe M, Ohtake M, Nakauchi Y, Tsumura K, Yabuta H, Ishihara Y, Noguchi R, Matsumoto K, Miura A, Namiki N, Tachibana S, Arakawa M, Ikeda H, Wada K, Mizuno T, Hirose C, Hosoda S, Mori O, Shimada T, Soldini S, Tsukizaki R, Yano H, Ozaki M, Takeuchi H, Yamamoto Y, Okada T, Shimaki Y, Shirai K, Iijima Y, Noda H, Kikuchi S, Yamaguchi T, Ogawa N, Ono G, Mimasu Y, Yoshikawa K, Takahashi T, Takei Y, Fujii A, Nakazawa S, Terui F, Tanaka S, Yoshikawa M, Saiki T, Watanabe S, Tsuda Y (2020) Sample collection from asteroid (162173) Ryugu by Hayabusa 2: implications for surface evolution. *Science* 368:654–659. <https://doi.org/10.1126/science.aaz6306>

- Ostro SJ, Pravec P, Benner LA, Hudson RS, Sarounova L, Hicks MD, Rabinowitz DL, Scotti JV, Tholen DJ, Wolf M, Jurgens RF, Thomas ML, Giorgini JD, Chodas PW, Yeomans DK, Rose R, Frye R, Rosema KD, Winkler R, Slade MA (1999) Radar and optical observations of asteroid 1998 KY26. *Science* 285:557–559
- Sato M, Watanabe J-I, Tanabe T, Ohnishi K, Ohkawa T, Iijima Y, Kagaya Y (2012) Observed magnitude and luminous efficiency of reentry capsule of HAYABUSA spacecraft. *Publ Astron Soc Jpn*. <https://doi.org/10.1093/pasj/64.2.41>
- Sato H, Robinson MS, Hapke B, Denevi BW, Boyd AK (2014) Resolved Hapke parameter maps of the Moon. *J Geophys Res Planets* 119(8):1775–1805. <https://doi.org/10.1002/2013JE004580>
- Sugita S, Honda R, Morota T, Kameda S, Sawada H, Tatsumi E, Yamada M, Honda C, Yokota Y, Kouyama T, Sakatani N, Ogawa K, Suzuki H, Okada T, Namiki N, Tanaka S, Iijima Y, Yoshioka K, Hayakawa M, Cho Y, Matsuoka M, Hirata N, Hirata N, Miyamoto H, Domingue D, Hirabayashi M, Nakamura T, Hiroi T, Michikami T, Michel P, Ballouz RL, Barnouin OS, Ernst CM, Schröder SE, Kikuchi H, Hemmi R, Komatsu G, Fukuhara T, Taguchi M, Arai T, Senshu H, Demura H, Ogawa Y, Shimaki Y, Sekiguchi T, Müller TG, Hagermann A, Mizuno T, Noda H, Matsumoto K, Yamada R, Ishihara Y, Ikeda H, Araki H, Yamamoto K, Abe S, Yoshida F, Higuchi A, Sasaki S, Oshigami S, Tsuruta S, Asari K, Tazawa S, Shizugami M, Kimura J, Otsubo T, Yabuta H, Hasegawa S, Ishiguro M, Tachibana S, Palmer E, Gaskell R, Le Corre L, Jaumann R, Otto K, Schmitz N, Abell P, Barucci MA, Zolensky ME, Vilas F, Thuillet F, Sugimoto C, Takaki N, Suzuki Y, Kamiyoshihara H, Okada M, Nagata K, Fujimoto M, Yoshikawa M, Yamamoto Y, Shirai K, Noguchi R, Ogawa N, Terui F, Kikuchi S, Yamaguchi T, Oki Y, Takao Y, Takeuchi H, Ono G, Mimasu Y, Yoshikawa K, Takahashi T, Takei Y, Fujii A, Hirose C, Nakazawa S, Hosoda S, Mori O, Shimada T, Soldini S, Iwata T, Abe M, Yano H, Tsukizaki R, Ozaki M, Nishiyama K, Saiki T, Watanabe S, Tsuda Y, (2019) The geomorphology, color, and thermal properties of Ryugu: implications for parent-body processes. *Science*. <https://doi.org/10.1126/science.aaw0422>
- Suzuki H, Yamada M, Kouyama T, Tatsumi E, Kameda S, Honda R, Sawada H, Ogawa N, Morota T, Honda C, Sakatani N, Hayakawa M, Yokota Y, Yamamoto Y, Sugita S (2018) Initial inflight calibration for Hayabusa2 optical navigation camera (ONC) for science observations of asteroid Ryugu. *Icarus* 300:341–359. <https://doi.org/10.1016/j.icarus.2017.09.011>
- Tachibana S, Sawada H, Okazaki R, Takano Y, Sakamoto K, Miura YN, Okamoto C, Yano H, Yamanouchi S, Michel P, Zhang Y, Schwartz S, Thuillet F, Yurimoto H, Nakamura T, Noguchi T, Yabuta H, Naraoka H, Tsuchiyama A, Imae N, Kurosawa K, Nakamura AM, Ogawa K, Sugita S, Morota T, Honda R, Kameda S, Tatsumi E, Cho Y, Yoshioka K, Yokota Y, Hayakawa M, Matsuoka M, Sakatani N, Yamada M, Kouyama T, Suzuki H, Honda C, Yoshimitsu T, Kubota T, Demura H, Yada T, Nishimura M, Yogata K, Nakato A, Yoshitake M, Suzuki AI, Furuya S, Hatakeda K, Miyazaki A, Kumagai K, Okada T, Abe M, Usui T, Ireland TR, Fujimoto M, Yamada T, Arakawa M, Connolly HC, Fujii A, Hasegawa S, Hirata N, Hirose C, Hosoda S, Iijima Y, Ikeda H, Ishiguro M, Ishihara Y, Iwata T, Kikuchi S, Kitazato K, Lauretta DS, Libourel G, Marty B, Matsumoto K, Michikami T, Mimasu Y, Miura A, Mori O, Nakamura-Messenger K, Namiki N, Nguyen AN, Nittler LR, Noda H, Noguchi R, Ogawa N, Ono G, Ozaki M, Senshu H, Shimada T, Shimaki Y, Shirai K, Soldini S, Takahashi T, Takei Y, Takeuchi H, Tsukizaki R, Wada K, Yamamoto Y, Yoshikawa K, Yumoto K, Zolensky ME, Nakazawa S, Terui F, Tanaka S, Saiki T, Yoshikawa M, Watanabe S, Tsuda Y (2022) Pebbles and sand on asteroid (162173) Ryugu: in situ observation and particles returned to Earth. *Science* 375:1011–1016. <https://doi.org/10.1126/science.abj8624>
- Tatsumi E, Kouyama T, Suzuki H, Yamada M, Sakatani N, Kameda S, Yokota Y, Honda R, Morota T, Moroi K, Tanabe N, Kamiyoshihara H, Ishida M, Yoshioka K, Sato H, Honda C, Hayakawa M, Kitazato K, Sawada H, Sugita S (2019) Updated inflight calibration of Hayabusa2's optical navigation camera (ONC) for scientific observations during the cruise phase. *Icarus* 325:153–195. <https://doi.org/10.1016/j.icarus.2019.01.015>
- Tatsumi E, Domingue D, Schröder S, Yokota Y, Kuroda D, Ishiguro M, Hasegawa S, Hiroi T, Honda R, Hemmi R, Le Corre L, Sakatani N, Morota T, Yamada M, Kameda S, Koyama T, Suzuki H, Cho Y, Yoshioka K, Matsuoka M, Honda C, Hayakawa M, Hirata N, Hirata N, Yamamoto Y, Vilas F, Takato N, Yoshikawa M, Abe M, Sugita S (2020) Global photometric properties of (162173) Ryugu. *Astron Astrophys* 639:A83. <https://doi.org/10.1051/0004-6361/201937096>
- Watanabe S, Hirabayashi M, Hirata N, Na H, Noguchi R, Shimaki Y, Ikeda H, Tatsumi E, Yoshikawa M, Kikuchi S, Yabuta H, Nakamura T, Tachibana S, Ishihara Y, Morota T, Kitazato K, Sakatani N, Matsumoto K, Wada K, Senshu H, Honda C, Michikami T, Takeuchi H, Kouyama T, Honda R, Kameda S, Fuse T, Miyamoto H, Komatsu G, Sugita S, Okada T, Namiki N, Arakawa M, Ishiguro M, Abe M, Gaskell R, Palmer E, Barnouin OS, Michel P, French AS, McMahon JW, Scheeres DJ, Abell PA, Yamamoto Y, Tanaka S, Shirai K, Matsuoka M, Yamada M, Yokota Y, Suzuki H, Yoshioka K, Cho Y, Tanaka S, Nishikawa N, Sugiyama T, Kikuchi H, Hemmi R, Yamaguchi T, Ogawa N, Ono G, Mimasu Y, Yoshikawa K, Takahashi T, Takei Y, Fujii A, Hirose C, Iwata T, Hayakawa M, Hosoda S, Mori O, Sawada H, Shimada T, Soldini S, Yano H, Tsukizaki R, Ozaki M, Iijima Y, Ogawa K, Fujimoto M, Ho T-M, Moussi A, Jaumann R, Bibring J-P, Krause C, Terui F, Saiki T, Nakazawa S, Tsuda Y (2019) Hayabusa2 arrives at the carbonaceous asteroid 162173 Ryugu? A spinning top shaped rubble pile. *Science*. <https://doi.org/10.1126/science.aav8032>
- Yamada T, Yoshihara T (2022) Post-Flight Analysis of Recovered Components of Hayabusa2 Sample Return Capsule. In: *International Symposium on Space Technology and Science*. https://archive.ists.or.jp/upload_pdf/E-1-05.pdf
- Yokota Y, Matsunaga T, Ohtake M, Haruyama J, Nakamura R, Yamamoto S, Ogawa Y, Morota T, Honda C, Saiki K, Nagasawa K, Kitazato K, Sasaki S, Iwasaki A, Demura H, Hirata N, Hiroi T, Honda R, Iijima Y, Mizutani H (2011) Lunar photometric properties at wavelengths 0.5–1.6 μm acquired by SELENE Spectral Profiler and their dependency on local albedo and latitudinal zones. *Icarus* 215(2):639–660. <https://doi.org/10.1016/j.icarus.2011.07.028>
- Yokota Y, Honda R, Tatsumi E, Domingue D, Schröder S, Matsuoka M, Morota T, Sakatani N, Kameda S, Kouyama T, Yamada M, Honda C, Hayakawa M, Cho Y, Michikami T, Suzuki H, Yoshioka K, Sawada H, Ogawa K, Yumoto K, Sugita S (2021) Opposition observations of 162173 Ryugu: normal albedo map highlights variations in regolith characteristics. *Planet Sci J*. <https://doi.org/10.3847/psj/ac14ba>

Publisher's Note

Springer Nature remains neutral with regard to jurisdictional claims in published maps and institutional affiliations.

Submit your manuscript to a SpringerOpen[®] journal and benefit from:

- Convenient online submission
- Rigorous peer review
- Open access: articles freely available online
- High visibility within the field
- Retaining the copyright to your article

Submit your next manuscript at ► [springeropen.com](https://www.springeropen.com)